Supplemental Information - Appendix

Core collection

Scientific drilling was completed in March and April 2005 using the Malawi Lake Services barge *Viphya*, which was extensively modified for this drilling effort. A summary of the Lake Malawi Drilling Project core recovery is shown in Table S1. Hole 1C over-penetrated the upper sedimentary section, and thus a 6.5 m shift was applied to Hole 1C. The top of Hole 1B was adjusted to 19.5 meters below lake floor (mblf), in agreement with the driller's logs.

Geochemical and geophysical analyses

The composite record from Site 1 was produced using drillers depth logs as well as density, L* values, and total organic carbon (TOC) records from both Holes 1B and 1C. Sample intervals vary among the geochemical and geophysical data sets at Drill Site 1 from millimeter-scale (L*) to 16 cm (TOC).

High-resolution digital imagery (pixel size is ~0.1 mm) of each core section was captured using a 1) DMT CoreScan Colour scanner and 2) a Geotek Geoscan-V scanner with polarizing filters on both the cameras and the light source at the National Lacustrine Core Repository (LacCore), University of Minnesota. To reduce total data volume, each image was resampled to 10% of its original size using the bicubic interpolation tool in Adobe Photoshop©, reducing sample intervals to ~1 mm. Red-Green-Blue (RGB) data were extracted from a 9-pixel-wide horizontal band from the center of each core section. RGB values from the imagery captured using the Geotek Geoscan-V scanner were calibrated to RGB values determined using the DMT CoreScan Colour scanner, by the use of a transform function generated from cross-plots of colors from calibration cards from the two sets of images. RGB space was then converted to L*, a*, b* space, where L* represents the lightness of color in the core image. To eliminate high-frequency variability due to small gaps and cracks (dark values) a filter was applied to the final data set, where a given point was eliminated if its L* value fell outside two standard deviations of a 100-point running mean. Calcium (Ca), a proxy for calcium carbonate mineral abundance, was measured in 1-cm intervals using an ITRAX X-ray Fluorescence Core Scanner at the Large Lakes Observatory of the University of Minnesota-Duluth. The cores were exposed to X-radiation generated by a molybdenum source set to 30 kV and 15 mA. XRF counts per minute (cpm) correspond to Ca concentrations in NIST Standard Reference Materials. The 1C part of record had twice the exposure time relative to 1B, so the 1C counts were reduced by 50%. Saturated bulk density measurements were taken every 1 cm using a Gamma-Ray Attenuation Porosity Evaluator (GRAPE) on a Geotek multi-sensor logger at LacCore. Organic matter samples for TOC and $\delta^{13}C$ were measured in 1-cm thick discrete samples at 16 cm intervals. They were pretreated with a vapor phase acidification (*S1*) technique to remove inorganic carbon

phases and then analyzed using an ANCA elemental analyzer and accelerator mass spectrometer at the University of Miami Stable Isotope Laboratory.

Age dating methodology

Age dating of the drill-core samples recovered from site GLAD7-Mal05-1 using drill cores from holes 1B and 1C was accomplished using several different dating methods. The principal ages for the GLAD7-Mal05-1 drill cores were obtained by using 16 AMS radiocarbon dates (0-21 m), the occurrence of the Toba Ash (28 m, 75 ka) (*S2*), Ar-Ar dates on two thin tephras (168m, 242 m), paleomagnetic reversal stratigraphy, and magnetic paleointensity (165 m to the base of the core) correlations to the global stack (Table S2). From these ages, we used a series of linked least-squared polynomials to develop an age model for the entire Site 1 record (Fig. S2).

AMS Radiocarbon and Toba Ash detection

The AMS radiocarbon dates are also detailed previously (*9*). Methods for the detection of the Toba ash are described in (*S2*).

Ar-Ar dating

Ar-Ar dating was completed at the Berkeley Geochronology Center. K-feldspar phenocrysts were separated from two thin tephra horizons for $^{40}Ar/^{39}Ar$ dating using the total-fusion approach. Analyses of sample GLAD7-MAL05 1B-54E (167.84 mblf) were carried out on six relatively small grains, resulting in an age with a relatively large uncertainty, 0.59 ± 0.02 Ma (1σ). Sample GLAD7-MAL05 1B-83E-3 (241.53 mblf) yielded much more material and a resulting higher precision age, 0.915 ± 0.008 Ma (n = 28).

K-feldspar phenocrysts were separated from tephra samples using gentle hand-crushing, followed by dilute HF (5%, 3 min) and distilled water rinses. Grains were hand-picked under binocular microscope, and irradiated in two separate batches in the Cd-lined, in-core CLICIT facility of the Oregon State University TRIGA reactor (sample GLAD7-MAL05 1B-83E-3 for 0.1 hour, and sample GLAD7-MAL05 1B-54E for 0.5 hour). Sanidine from the Alder Creek Rhyolite was used as a mineral standard to evaluate neutron fluence, with a reference age of 1.202 ± 0.012 Ma (*S3*) adjusted for the FC age of 28.201 ± 0.046 Ma (*S4*). Standards and unknowns were placed in 2-mm diameter by 2-mm deep wells situated in a ring configuration centered on the 16.5 mm diameter, 2.5 mm thick aluminum disk (*S5*). Planar regressions were fit to the standard data and the $^{40}Ar/^{39}Ar$ neutron fluence parameter, J, interpolated for the unknowns. Uncertainties in J (0.2–0.3%) are estimated based on Monte Carlo error analysis of the planar regressions. Reactor-induced isotopic production ratios for these irradiations were:

($^{36}Ar/^{37}Ar$)Ca = 2.65 ± 0.02 × 10^{-4}, ($^{38}Ar/^{37}Ar$)Ca = 1.96 ± 0.08 × 10^{-5}, ($^{39}Ar/^{37}Ar$) Ca = 6.95 ± 0.09 × 10^{-4}, ($^{37}Ar/^{39}Ar$) K = 2.24 ± 0.16 × 10^{-4}, ($^{38}Ar/^{39}Ar$) K = 1.220 ± 0.003 × 10^{-2}, ($^{40}Ar/^{39}Ar$) K = 2.5 ± 0.9 × 10^{-4}. The ^{40}K decay constants applied to age calculations were $\lambda\varepsilon$ = 5.810 ± 0.170 × 1011/yr and $\lambda\beta$ = 4.962 ± 0.086 × 1010/yr (*S6*).

Following irradiation, single-crystal total-fusion analyses were performed at the Berkeley Geochronology Center using a Noblesse 5-collector Noble gas mass spectrometer and dedicated extraction line. Individual K-feldspar phenocrysts ~0.2–0.5 mm in maximum dimension (est. ~10–130 micrograms) were heated for 5-7 seconds to fusion in UHV using a CO_2 laser at ~6 Watts with a 1.5 mm beam diameter. Evolved gasses were then exposed for ~60 seconds to a 50 cc SAES getter operated at 2.1 A and a cryosurface at -125°C to remove reactive species and water. The gas was then admitted to the mass spectrometer and measured by ion counting over a period of about eight minutes. This machine has ETP (Model 14143) ion counters at differential spacing of 1 and 2 m/e both above and below an axial Faraday cup, a configuration that permits simultaneous measurement of ^{40}Ar, ^{39}Ar, ^{37}Ar, and ^{36}Ar on individual ion counters. A brief peak hop was employed several times during the run to allow ^{38}Ar to be measured on one of the ion counters. All electronic source and detector settings were held constant for the duration of mass spectrometry. ^{36}Ar signals were normalized to the detector used for the ^{40}Ar and ^{39}Ar measurements by reference to relative gains evaluated by time-interpolation through periodic runs of atmospheric argon measured using the same source and detector settings as the unknowns (1–2 air runs every ~15 analyses; ^{40}Ar delivered to the mass spectrometer per air aliquot = 2.5 X 10-15 moles; $^{40}Ar/^{36}Ar$ = 298.56 ± 0.31; (*S7*)). Normalization of ^{39}Ar, ^{38}Ar and ^{37}Ar signals were achieved by using the same air shots using a post-run test sequence invoking repeated measurement of ^{40}Ar on relevant detectors. Procedural blanks bracketed every total-fusion analysis, and yielded approximately 5 × 10^{-17}, 9 × 10^{-19}, 3 × 10^{-19}, 7 × 10^{-18}, and 6 × 10^{-19} moles of at the measurement positions of ^{40}Ar, ^{39}Ar, ^{38}Ar, ^{37}Ar, and ^{36}Ar, respectively.

Sample GLAD7-MAL05 1B-54E yielded only six K-feldspar crystals sufficiently large for analysis. Although all extractions were highly radiogenic (yielding >75%, mostly >90% radiogenic ^{40}Ar), the small grain size and relatively young age resulted in large age uncertainties, from 5-40%. The probability density function of the results are shown below (Fig. S3). The observed distribution is sub-gaussian, with a slight skewing toward older ages, though the MSWD remains reasonable (0.78). The weighted-mean age of the six analyses is 0.59 ± 0.02 Ma (1σ analytical error). The high radiogenic content of the analyses precludes effective isochron correlation analysis, though for reference these data yield an inverse $^{36}Ar/^{40}Ar$ vs. $^{39}Ar/^{40}Ar$ isochron age of 0.58 ± 0.08 Ma, in agreement with the weighted-mean age, and a poorly defined $^{40}Ar/^{36}Ar$ intercept of 1,000 ± 1,700.

Sample GLAD7-MAL05 1B-83E-3 yielded many more grains for analysis (n = 37) than the previous sample. The geochronological data are displayed in Fig. S4. While most analyses yielded >75% ^{40}Ar*, six ranged from 14–64%, and may represent altered material (most of these also have relatively young ages). These are considered anomalous and excluded from further data analysis. The remaining population has a simple unimodal distribution but with a small shoulder of older ages. Tails toward older ages are often seen in single-crystal total-fusion analyses of late Cenozoic feldspars, and may represent excess ^{40}Ar present in glass inclusions in some crystals. A robust outlier filter, eliminating grains with ages more than 2.0 nMads

(normalized deviations from the median) was employed to trim the population, resulting in removal of three analyses from the data set. The resulting analyses give a weighted-mean age of 0.915 ± 0.006 Ma (MSWD = 1.3, n = 28). For reference, an isochron from these data yields an age of 0.900 ± 0.008 Ma (MSWD = 0.81, ($^{40}Ar/^{36}Ar$) int = 394 ± 35), within 2σ error of the weighted-mean age. Analytical results are presented in Table S3.

Paleomagnetic analyses

To incorporate the paleomagnetic data, we employed an iterative approach of interpreting both the inclination and paleo-intensity records:

1) Used Ar-Ar dates to constrain first-order absolute age model "pins" for the full Site 1 record (from 165 to 384 m below lake floor).

2) Measured inclination and relative paleointensity for Site 1 (1B).

3) Identified major reversals and excursions in the inclination record (Fig. S5): Bruhnes/Matayama boundary =222 m; Santa Rosa = 247 m; Upper Jaramillo = 271.5 m.

4) Following the establishment of the reversal stratigraphy, magnetic paleointensity was interpreted between the younger Ar-Ar date (~165 m) and the base of the core, with supporting interpretations from the inclination data. Magnetic paleointensity was determined from the ratio of natural remnant magnetization to anhysteretic remnant magnetization (NRM/ARM) (a measure of magnetic field intensity), were correlated to the global paleointensity stack) (*S8*). Excursions in the paleomagnetic inclination record (Fig. S6) were identified using classifications from (*S9, S10*).

PCA Computation and lake-level calibration

In order to determine trends in lake-level indicators from drill-core analyses, principal component analysis (PCA) was performed on density, TOC, $\delta^{13}C$, Ca, and L* (Fig. S1). Total organic carbon is most sensitive during times of high and intermediate lake level, $\delta^{13}C$ is more sensitive to lake level variability during times of very low lake level, and Ca is sensitive during times of intermediate and low lake level. Density and L* are physical properties used to quantify lithology which varies with water depth at the drill site. Variables contributing to PCA were re-sampled to the lowest resolution data set (TOC) using an integration technique in Analyseries©. The first principal component (PC(1)) represents 49% of the total variance and the weights from all contributing variables are between 0.31 and 0.54.

Seismic facies analysis and paleo-ecological indicators pinpoint lowstand magnitudes at Site 1 for several intervals over the last ~200,000 years (*9, 17, 18*). We plot PC(1) against these

lowstand magnitudes to generate a transform function to calibrate lake level over the entire Site 1 record (Fig. S7). This calibration is used to assess lowstand magnitudes throughout the late Quaternary (Fig. S7). Note that lowstands interpreted from seismic-reflection data reflect intervals of sustained lower lake level and not necessarily the most extreme, short-term events. However, the paleo-ecological data sets are higher resolution and can define higher frequency events.

Calibration of seismic facies

Interpretations of seismic facies from the paleo-shoreline of the most recent (centered at ~145 ka) -500 m lowstand surface (*9, 17*) indicate that rocky coastlines during lowstands are associated with a faulted, high-amplitude seismic-reflection character (Fig. 3, S8). Interpreted sandy coastlines have high-amplitude, continuous reflections while interpreted mixed mud/sand vegetated coastlines are characterized by low-amplitude, continuous reflections (Fig. S8). Interpretations of sandy coastline are supported by drill-core and seismic-reflection data at Drill Site 2 in Lake Malawi, where fine- to medium-grained sand found at the base of the drill core is interpreted as a transgressive beach deposit in the drill cores (Fig. S8) (*9*). This fining-upwards sedimentary package is associated with high-amplitude, continuous reflections in seismic data (*17*).

Presentation of TRMM results

A 12-year (1998 – 2010) processed compilation of NASA's Tropical Rainfall Measuring Mission (TRMM) data for January and July were downloaded from B. Bohagen (http://www.geog.ucsb.edu/~bodo/TRMM/) to be used in Fig. 1 (*S11)*. Combined Precipitation Radar (PR) and TRMM Microwave Imager (TMI) were used on product 2B31 with 4 km horizontal and 250 m vertical resolution.

Supplemental Figures:

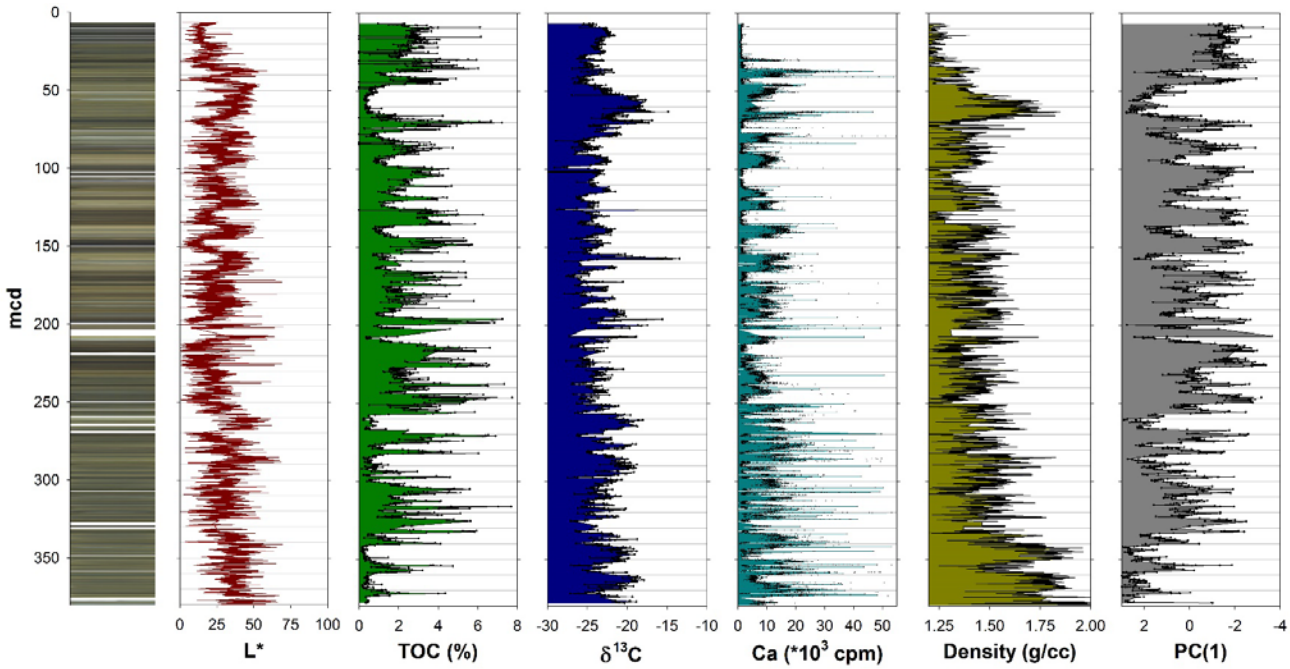

Fig. S1. Paleoclimate proxy records used in the Principal Component Analysis. Vertical axis mcd = meters composite depth from all holes at site. Column on left is condensed high-resolution core image of all composited core from Site 1. See Suppl. Text.

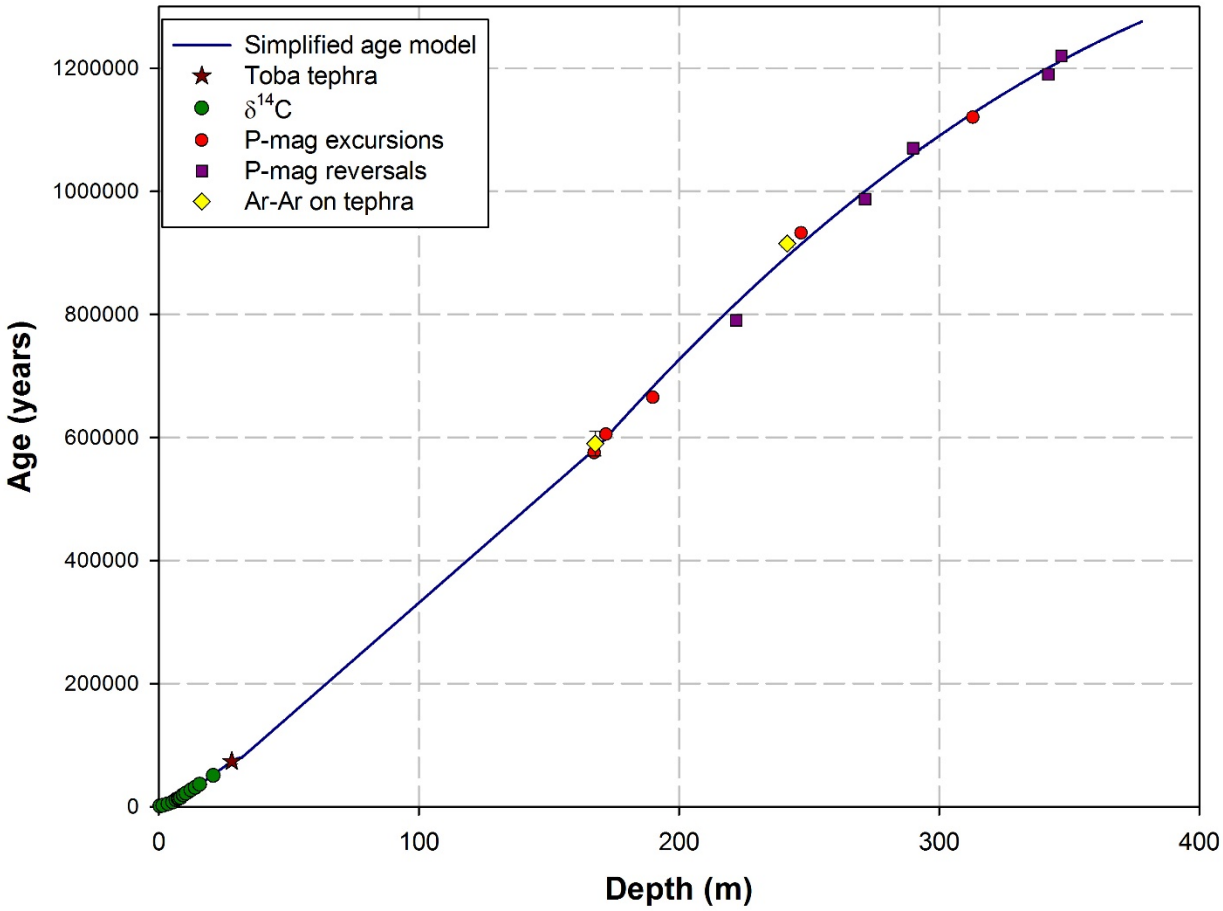

Fig. S2. Age-depth relationships for the Lake Malawi Drilling Project Site 1, illustrating dates and age model approaches employed. The age model (blue solid line) is used to transform paleoclimate proxies, including PC(1), to age from depth, as presented in the main text.

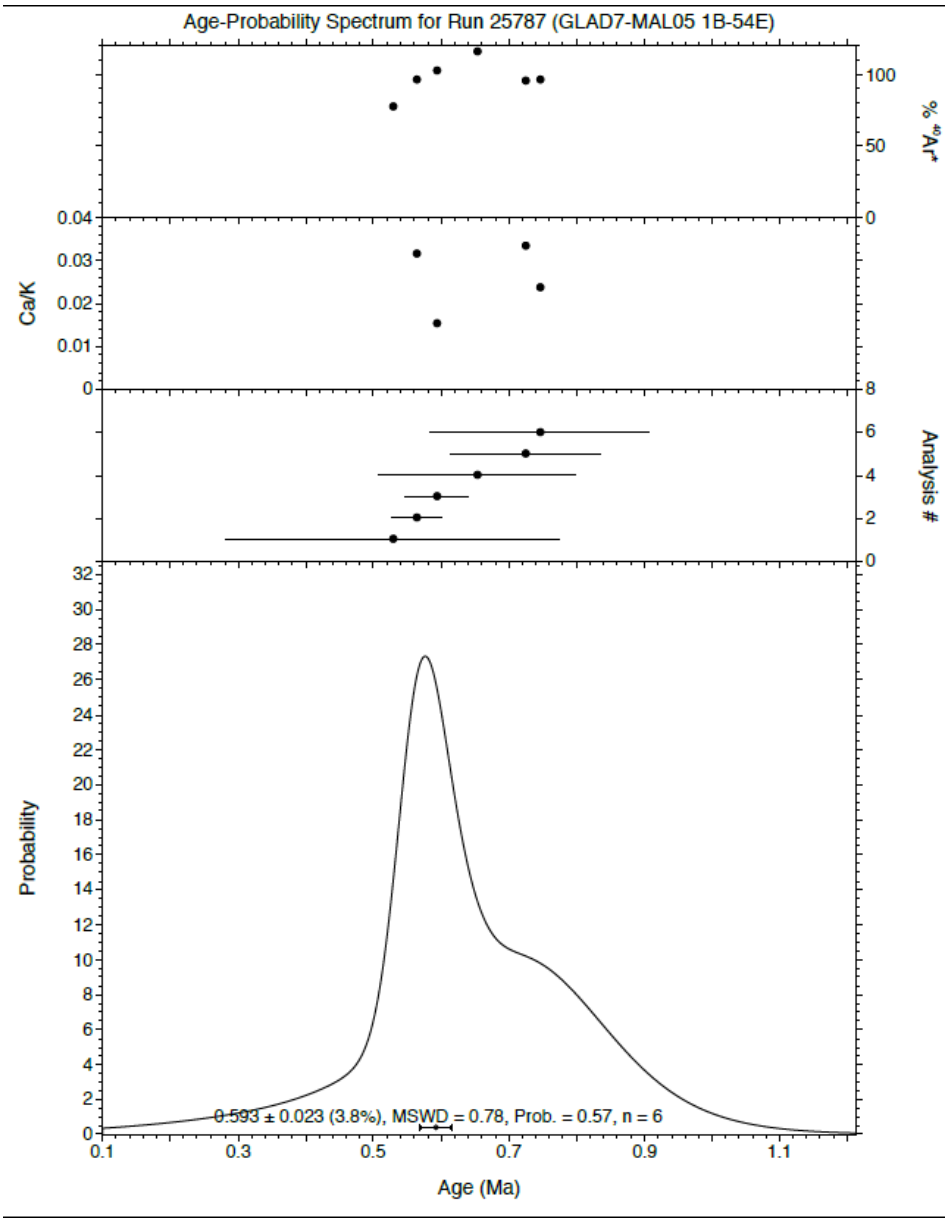

Fig. S3. Probability density function for sample GLAD7-MAL05 1B-54E.

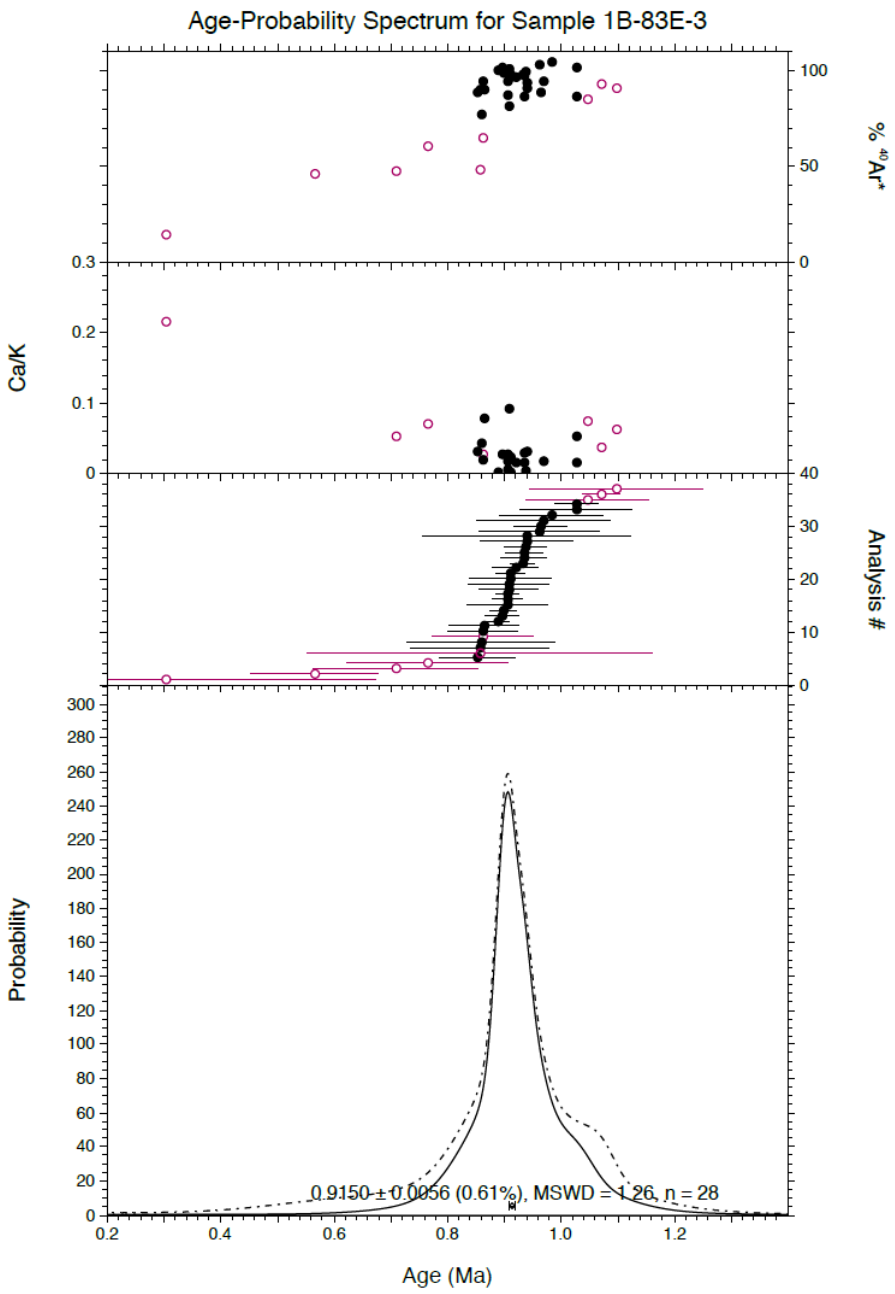

Fig. S4. Probability density function for sample GLAD7-MAL05 1B-83E-3.

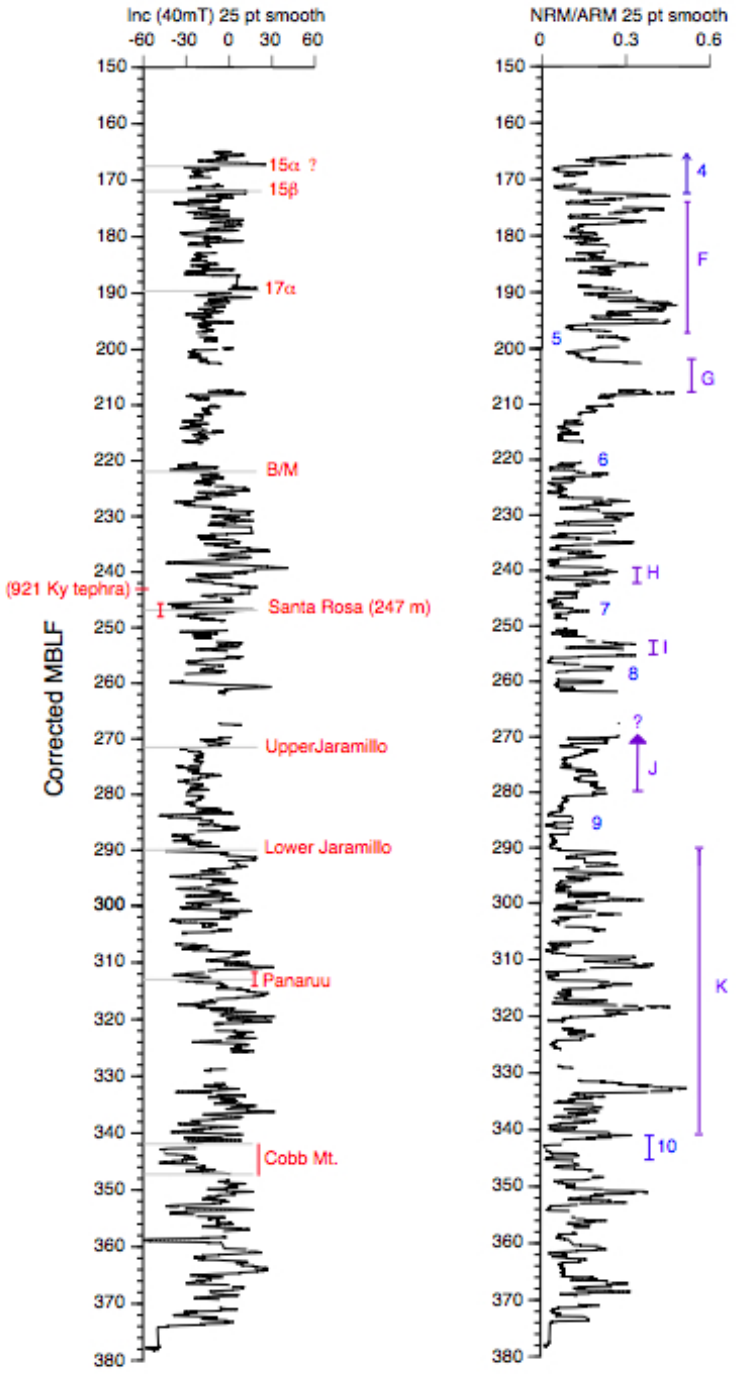

Fig. S5. Inclination and paleointensity data for Malawi core 1B. The inclination record was demagnetized at 50 mT with a 50-point smooth. Geomagnetic excursions (sharp changes to positive values) are identified using classification from (*S8*). Here, the paleomagnetic intensity record is shown correlated to global composite paleointensity record SINT-2000 (*S9*).

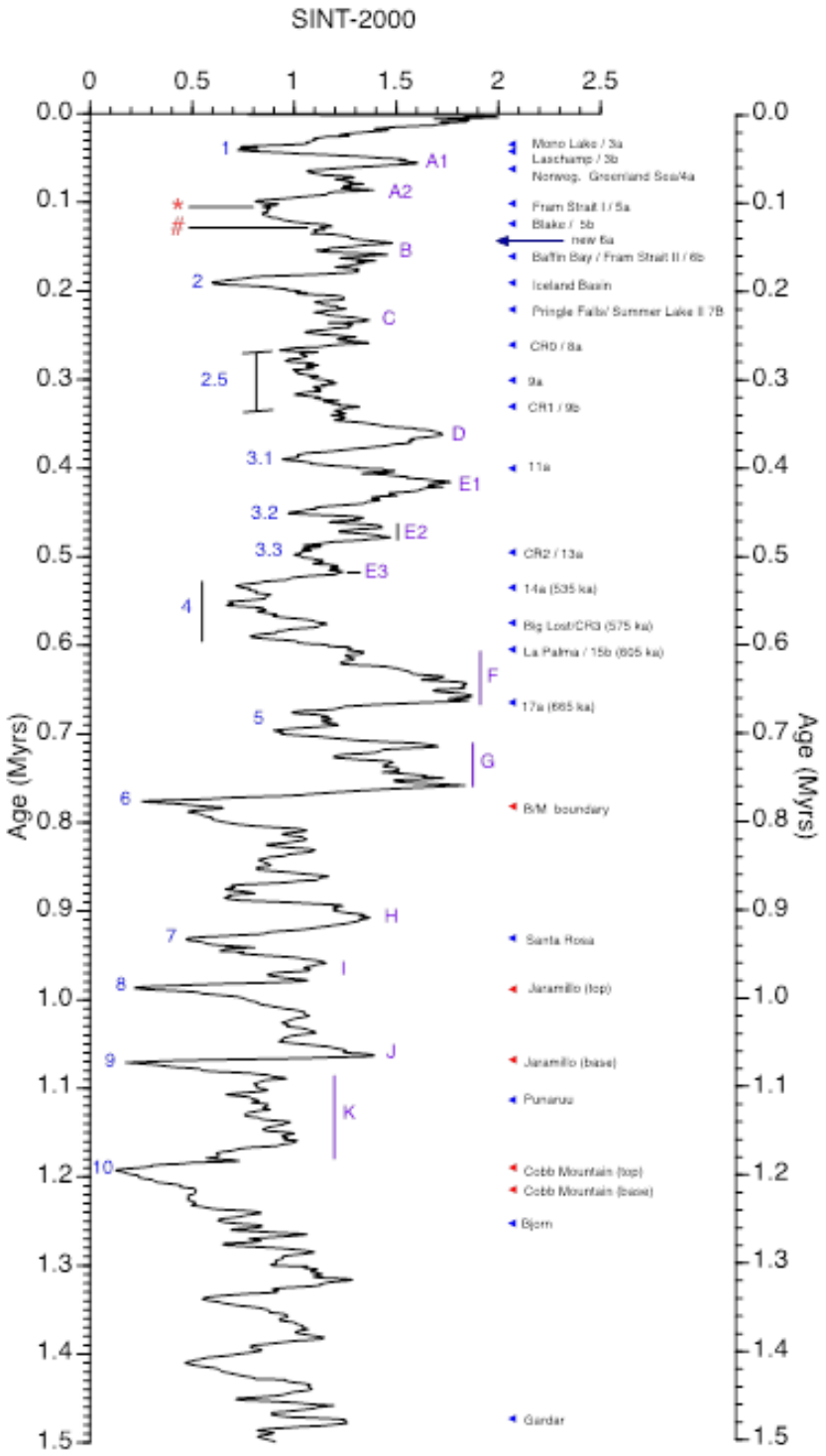

Fig. S6. The SINT-2000 paleointensity stack (*S8*) with locations of excursions and reversals in the record (*S8, S9*). The numbered and lettered paleointensity features are identified in the Malawi record shown in Fig. S5.

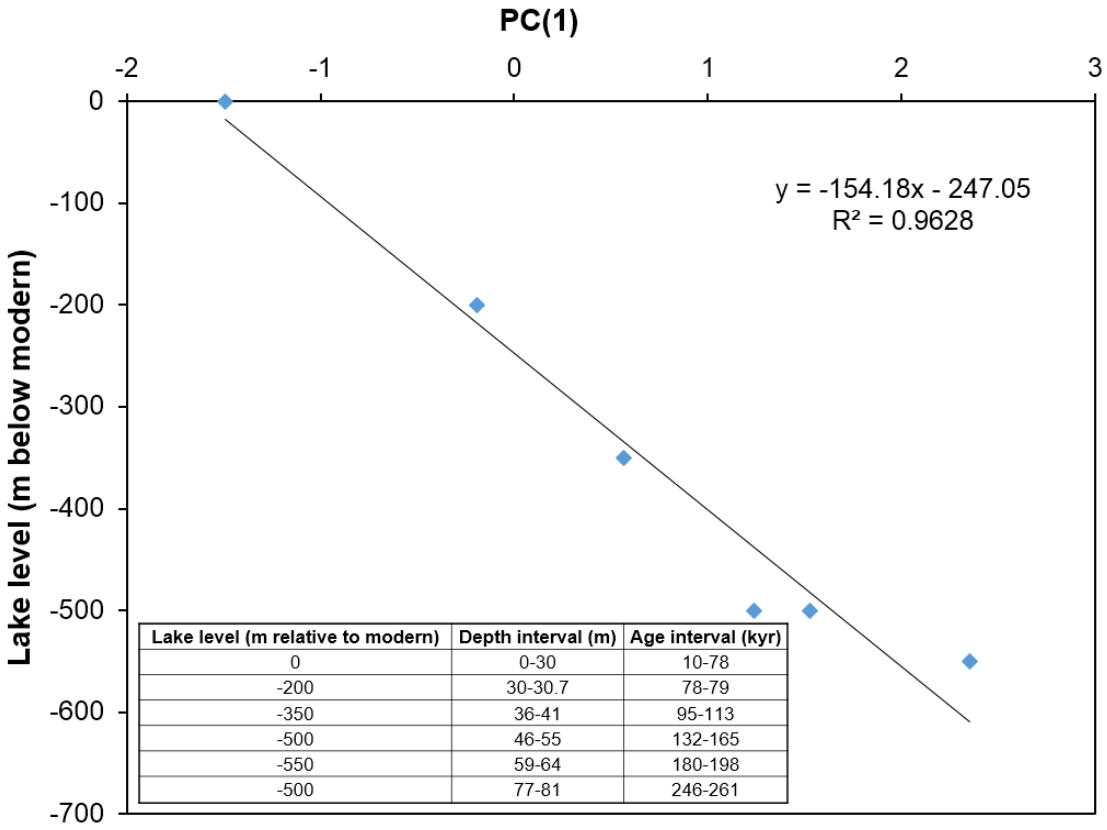

Lake level (m relative to modern)	Depth interval (m)	Age interval (kyr)
0	0-30	10-78
-200	30-30.7	78-79
-350	36-41	95-113
-500	46-55	132-165
-550	59-64	180-198
-500	77-81	246-261

Fig. S7. Calibration of PC(1) lake level with seismic lowstand indicators (plot of lowstand magnitude vs. PC(1) values). Intervals of known lowstand magnitudes from seismic facies and paleo-ecological data are shown in the inserted table.

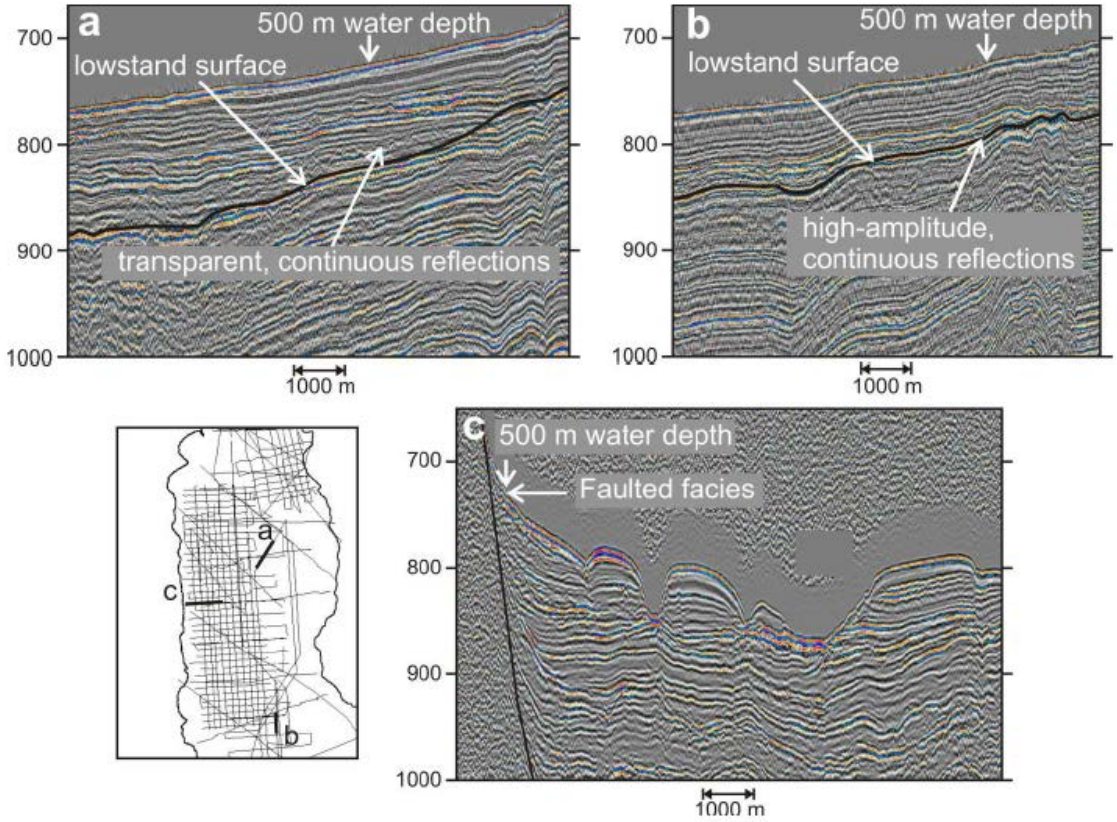

Fig. S8. Interpretations of seismic facies from the paleo-shoreline of the most recent (~145 kyr) -500 m lowstand surface and megadrought interval (*9*, *17*). (a) A seismic profile showing low-amplitude continuous reflections, interpreted as a mixed-vegetative lowstand coastline. (b) The -500 m lowstand surface is characterized by high-amplitude continuous reflections, indicative of a sandy lowstand surface. (c) The seismic-profile shows the -500 m lowstand water depth is associated with a fault-scarp, indicative of a rocky lowstand coastline during the lowstand.

Site	Latitude	Longitude	Water depth (m)	Hole	Maximum depth below lake floor (m)
Glad7-Mal05-1	11° 17' 38" S	34° 26' 14" E	590	A	38.57
				B	379.29
				C	88.89
				D	23.82
Glad7-Mal05-2	10° 1' 4" S	34° 11' 10" E	359	A	38.81
				B	39.85
				C	36.96

Table S1. Drilling program summary

Hole	Depth (m)	Type of date	Calendar Age (kyr BP)	± Error (kyr)	Methodology	Magnetic features
1C	0.56	^{14}C	0.82	0.07	CALPAL	
1C	1.7	^{14}C	1.77	0.05	CALPAL	
1C	3.71	^{14}C	4.27	0.1	CALPAL	
1C	5.46	^{14}C	7.14	0.09	CALPAL	
1C	6.71	^{14}C	11.01	0.14	CALPAL	
1C	7.51	^{14}C	12.63	0.08	CALPAL	
1C	7.9	^{14}C	13.33	0.15	CALPAL	
1C	8.51	^{14}C	14.57	0.31	CALPAL	
1C	9.46	^{14}C	18.45	0.22	CALPAL	
1C	9.56	^{14}C	18.8	0.18	CALPAL	
1C	11.52	^{14}C	23.97	0.27	CALPAL	
1C	10.55	^{14}C	21.53	0.47	CALPAL	
1C	12.46	^{14}C	26.59	0.43	CALPAL	
1C	14.09	^{14}C	30.89	0.21	CALPAL	
1C	15.81	^{14}C	36.14	0.42	CALPAL	
1C	21.05	^{14}C	50.46	3.24	CALPAL	
1C	28.09	Toba Ash	73.5	4		
1B	167.84	Ar-Ar	590	20		
1B	241.63	Ar-Ar	915	6		
1B	167.5	Excursion	~575		Lund	15a
1B	172	Excursion	605		Lund	15B
1B	190	Excursion	665		Lund	17a
1B	222	Reversal	790		Lund	Brunhes-Matuyama
1B	247	Excursion	932		Lund	Santa Rosa
1B	271.5	Reversal	987		Lund	Upper Jaramillo
1B	290	Reversal	1070		Lund	Lower Jaramillo
1B	313	Excursion	1120		Lund	Punaruu
1B	342	Reversal	1190		Lund	Cobb Mountain
1B	347	Reversal	1220		Lund	Cobb Mountain

Table S2. Age-depth data for Malawi Site 1, Holes 1B and 1C.

Lab ID#	J		Relative Isotopic Abundances										Derived Results						
			^{40}Ar		^{39}Ar		^{38}Ar		^{37}Ar		^{36}Ar		^{39}Ar Mo	Ca/K		$\%^{40}Ar^{*}$	Age (Ma)		w/±J
	(X 10^{-3})	± 1σ		±1σ		±1σ		±1σ		±1σ		±1σ	∞ 10^{-15}		±1σ			±1σ	
GLAD7-MAL05 1B-83E-3																			
25583-01	0.02720	0.00005	20540	100	747	4	0.308	0.016	4.8	1.7	25	4	0.007	0.026	0.009	64.1	0.86	0.08	0.08
25583-02	0.02720	0.00005	70780	80	3324	9	0.131	0.016	3.9	1.7	31	2	0.029	0.004	0.002	87.0	0.908	0.012	0.01
25583-03	0.02720	0.00005	29850	70	1340	6	0.103	0.020	9.3	1.7	14	3	0.012	0.028	0.005	85.8	0.94	0.03	0.03
25583-04	0.02720	0.00005	27670	60	1401	6	0.104	0.017	5.0	1.8	3	2	0.012	0.014	0.005	96.9	0.94	0.02	0.02
25583-05	0.02720	0.00005	19540	50	1005	5	0.000	0.018	0.8	1.8	1	2	0.009	0.003	0.007	98.5	0.94	0.03	0.03
25583-06	0.02720	0.00005	39860	60	2077	7	0.000	0.016	11.3	1.7	4	2	0.018	0.022	0.003	97.1	0.913	0.016	0.02
25583-07	0.02720	0.00005	47520	70	2597	8	0.000	0.018	0.4	1.7	1	2	0.023	0.000	0.003	99.3	0.890	0.013	0.01
25583-08	0.02720	0.00005	26740	60	1473	6	0.153	0.016	9.2	1.7	0	2	0.013	0.026	0.005	101.0	0.90	0.02	0.02
25583-09	0.02720	0.00005	5930	40	307	3	0.000	0.015	0.0	1.7	0	2	0.003	0.00	0.02	102.1	0.96	0.10	0.10
25583-10	0.02720	0.00005	13390	50	726	4	0.000	0.017	0.0	1.7	0	2	0.006	0.000	0.010	100.6	0.91	0.04	0.04
25583-11	0.02720	0.00005	5940	40	234.2	1.7	0.000	0.016	4.2	1.8	3.1	1.6	0.002	0.07	0.03	84.4	1.05	0.10	0.10
25583-12	0.02720	0.00005	21700	60	1111	5	0.000	0.016	3.9	1.7	3	2	0.010	0.014	0.006	96.3	0.92	0.03	0.03
25583-13	0.02720	0.00005	11110	50	592	4	0.046	0.019	2.8	1.7	2	2	0.005	0.019	0.012	94.1	0.86	0.05	0.05
25583-14	0.02720	0.00005	10660	50	551	4	0.18	0.02	0.1	1.8	1	2	0.005	0.000	0.014	96.3	0.91	0.06	0.06
25583-15	0.02720	0.00005	23440	50	992	5	0.113	0.017	8.6	1.8	5.8	1.6	0.009	0.036	0.008	92.6	1.07	0.02	0.03
25583-16	0.02720	0.00005	9410	40	455	4	0.115	0.018	3.4	1.8	2	2	0.004	0.031	0.017	92.8	0.94	0.07	0.07
25583-17	0.02720	0.00005	47120	60	2514	8	0.046	0.018	0.0	1.8	3	2	0.022	0.000	0.003	98.1	0.902	0.013	0.01
25583-18	0.02720	0.00005	20760	50	926	5	0.000	0.019	0.0	1.8	8	2	0.008	0.000	0.008	87.9	0.97	0.04	0.04
25583-19	0.02720	0.00005	48260	70	2466	7	0.16	0.02	0.0	1.8	4	2	0.022	0.000	0.003	97.4	0.934	0.013	0.01
25583-20	0.02720	0.00005	9740	40	495	4	0.00	0.02	3.1	1.8	2	2	0.004	0.026	0.015	94.0	0.91	0.06	0.06
25583-21	0.02720	0.00005	30900	60	1660	6	0.00	0.02	6.8	1.7	0	2	0.015	0.017	0.004	99.4	0.907	0.018	0.02
25583-22	0.02720	0.00005	10260	40	518	3	0.43	0.04	3.9	1.8	4	2	0.005	0.031	0.015	87.9	0.85	0.06	0.06
25583-23	0.02720	0.00005	7080	40	366	3	0.187	0.020	0.0	1.7	0	2	0.003	0.000	0.020	104.0	0.98	0.08	0.08
25583-24	0.02720	0.00005	7040	40	339	3	0.000	0.018	4.2	1.7	0	2	0.003	0.05	0.02	101.1	1.03	0.09	0.09
25583-26	0.02720	0.00005	7290	50	346	3	0.204	0.018	1.4	1.8	1	2	0.003	0.02	0.02	94.1	0.97	0.11	0.11
25583-27	0.02720	0.00005	5960	40	239.0	1.9	0.188	0.019	3.5	1.8	2	2	0.002	0.06	0.03	90.0	1.10	0.14	0.14
25583-28	0.02720	0.00005	12860	50	649	4	0.000	0.019	10.8	1.7	5	2	0.006	0.077	0.012	89.3	0.87	0.05	0.05
25583-29	0.02720	0.00005	13850	100	451	4	0.404	0.020	5.1	1.7	24	4	0.004	0.052	0.018	47.3	0.71	0.14	0.14
25583-30	0.02720	0.00005	15050	100	590	4	0.304	0.019	0.0	1.7	28	4	0.005	0.000	0.013	45.4	0.57	0.10	0.11
25583-31	0.02720	0.00005	7330	90	166	2	0.388	0.018	7.7	1.7	21	4	0.001	0.21	0.05	14.2	0.3	0.4	0.36
25583-32	0.02720	0.00005	20530	50	838	3	0.000	0.016	2.9	1.7	9.8	1.6	0.007	0.016	0.010	85.8	1.03	0.03	0.03
25583-33	0.02720	0.00005	6420	50	280	3	0.000	0.017	2.5	1.7	5	2	0.002	0.04	0.03	76.6	0.86	0.12	0.12
25583-34	0.02720	0.00005	9920	70	379	3	0.241	0.020	5.7	1.6	13	3	0.003	0.070	0.020	59.8	0.77	0.13	0.13
25583-35	0.02720	0.00005	5560	40	284	3	0.000	0.018	0.0	1.7	2	2	0.003	0.00	0.03	89.5	0.86	0.11	0.11
25583-36	0.02720	0.00005	17020	70	741	4	0.095	0.018	14.7	1.7	11	3	0.007	0.092	0.011	80.8	0.91	0.06	0.06
25583-37	0.02720	0.00005	4090	40	192	2	0.000	0.016	0.0	1.6	1	2	0.002	0.00	0.04	90.2	0.94	0.17	0.17
25583-39	0.02720	0.00005	4720	50	130	2	0.000	0.018	0.0	1.6	8	3	0.001	0.00	0.06	48.1	0.8	0.3	0.30
GLAD7-MAL05 1B-54E																			
25787-01	0.13980	0.00040	2490	60	1111	7	10	16	0	3	0.0	2.0	0.0010	0	0.018	115.9	0.65	0.14	0.14
25787-02	0.13980	0.00040	10440	50	4470	9	74	14	24	3	0.9	1.8	0.0039	0.032	0.004	97.5	0.57	0.03	0.03
25787-03	0.13980	0.00040	7380	50	3206	8	31	12	8	3	0.0	1.8	0.0028	0.015	0.005	102.6	0.6	0.04	0.04
25787-04	0.13980	0.00040	4020	50	1328	5	11	9	7	3	0.6	1.8	0.0012	0.033	0.013	95.2	0.73	0.1	0.10
25787-05	0.13980	0.00040	2730	50	886	5	0	12	3	3	0.3	1.8	0.0008	0.024	0.019	96.3	0.75	0.15	0.15
25787-06	0.13980	0.00040	1600	50	584	4	0	17	0	3	1.2	1.9	0.0005	0	0.03	76.9	0.5	0.2	0.24

Table S3. Ar-Ar analyses of Malawi tephras.

References in Supplemental Information

S1. Harris D, Horwáth WR, Van Kessel C (2001) Acid fumigation of soils to remove carbonates prior to total organic carbon or carbon-13 isotopic analysis. Soil Science Society of America Journal 65:1853-1856.

S2. Lane CS, Chorn BT, Johnson TC (2013) Ash from the Toba supereruption in Lake Malawi shows no volcanic winter in East Africa at 75 ka. Proceedings of the National Academy of Sciences 110: 8025–8029.

S3. Renne PR, et al. (1998) Intercalibration of standards, absolute ages and uncertainties in 40Ar/39Ar dating. Chemical Geology 145:117–152.

S4. Kuiper KF, et al. (2008) Synchronizing Rock Clocks of Earth History. Science 320:500-504.

S5. Best MG, Christiansen EH, Deino AL, Grommé CS, Tingey DG (1995) Correlation and emplacement of a large, zoned, discontinuously exposed ash flow sheet; the 40Ar/39Ar

chronology, paleomagnetism, and petrology of the Pahranagat Formation, Nevada. J. Geophys. Res., 100(B12):24593–24609, doi:10.1029/95JB01690.

S6. Steiger RH, Jäger E (1977) Subcommission on Geochronology: Conventions on the use of decay constants in geo- and cosmochronology. Earth Planet. Sci. Lett. 36:359-362.

S7. Lee J-Y, et al. (2006) A redetermination of the isotopic abundances of atmospheric Ar. Geochim. Cosmochim. Acta 70:4507–4512.

S8. Valet J-P, Meynadier L, Guyodo Y (2005) Geomagnetic dipole strength and reversal rate over the past two million years. Nature 435:802-805.

S9. Lund S, Stoner JS, Channell JET, Acton G (2006) A summary of Brunhes paleomagnetic field variability recorded in Ocean Drilling Program cores. Physics of the Earth and Planetary Interiors 156:194-204.

S10. Horng C-S, et al., (2002) Astronomically calibrated ages for geomagnetic reversals within the Matuyama chron. Earth Planets Space 54:679-690.

S11. Bookhagen B, Burbank DW (2010) Toward a complete Himalayan hydrological budget: Spatiotemporal distribution of snowmelt and rainfall and their impact on river discharge. Geophys. Res. Lett. 115:DOI: 10.1029/2009JF001426.